GPS Solutions (2018) 22:65
https://doi.org/10.1007/s10291-018-0732-z

ORIGINAL ARTICLE

Design and experimental evaluation of indirect centralized and direct decentralized integration scheme for low-cost INS/GNSS system

Hossein Nourmohammadi[1] · **Jafar Keighobadi**[1]

Received: 1 November 2017 / Accepted: 17 April 2018

Abstract
Advances in Geomatics science and technologies such as global navigation satellite system (GNSS) as well as inertial navigation system (INS) make it possible to develop accurate navigation system relying on low-cost technologies. We concentrated on integrated INS/GNSS system as a significant development in modern navigation systems. The ultimate aim is to enhance the performance, reliability, and navigation accuracy of low-cost INS/GNSS system. To achieve this, we focus on configuration and integration mechanization in low-cost INS/GNSS system. Two configurations, called here indirect centralized (IC) and direct decentralized (DD) integration, are proposed and a detailed comparative evaluation of the proposed schemes is provided. A serious problem of the low-cost INS/GNSS is the system reliability during GNSS signal blockage. Based on motion velocity constraints, the auxiliary velocity-update approach is proposed to enhance the navigation accuracy during GNSS outages. The assessment of the proposed integration schemes is conducted in numerous land/flight tests in which the host vehicle undergoes different dynamical maneuverings. Experimental evaluation shows that the IC integrated INS/GNSS has better performance in orientation estimation, but DD integrated INS/GNSS results in better positioning accuracy.

Keywords Low-cost INS/GNSS · Indirect centralized integration · Direct decentralized integration · MEMS-grade IMU · State estimation

Introduction

Global demands to achieve the highest possible precision in navigation while simultaneously having the lowest cost, bring about noticeable progresses in low-cost integrated inertial navigation systems (INSs). Based on micro-electro mechanical system (MEMS) technology, a new generation of low-cost inertial measurement units (IMUs) containing three-axis MEMS gyroscopes and accelerometers have been developed as the main components of commercial inertial navigation system. MEMS-grade inertial sensors are influenced by uncertainties comprising bias instabilities and stochastic noises (Doostdar and Keighobadi 2012). Despite of these uncertainties and errors, the output of inertial sensors is usually considered as genuine specific forces and angular rates in navigation computations of the strap-down INS. Additionally, during the inertial navigation computations, accelerometers bias and gyroscopes drift are integrated twice and three times, respectively. Therefore, the navigation error of the stand-alone INS rapidly enlarges with time (Hwang et al. 2005). As a matter of this fact, for long-term applications, the INS should be integrated with an aiding navigation system such as global navigation satellite system (GNSS). The GNSS provides drift-free position components that can be used to compensate the navigation error of the INS. On the other hand, the GNSS suffers from some limitations such as low update rate, signal blockage and especially lack of attitude angles determination. Therefore, the two systems have very complementary properties and are often employed together as an integrated INS/GNSS navigation system. Owing to covering the defects of individual INS and GNSS, the integrated INS/GNSS generates more reliable and accurate navigation data.

Integration mechanization plays a key role in the performance and accuracy of INS/GNSS navigation systems. Particularly, when low-cost MEMS-grade IMU is used in the INS, special approaches are required for the integration of GNSS with strap-down INS. Much research have been addressed in literature concerning low-cost integrated

✉ Hossein Nourmohammadi
hnourmohammadi@tabrizu.ac.ir

[1] Department of Mechanical Engineering, University of Tabriz, 29 Bahman, Tabriz 5166614766, Iran

Published online: 24 April 2018

inertial navigation systems. For example, Nassar and El-Sheimy (2006) enhanced the INS error model using autoregressive processes for modeling inertial sensor errors instead of Gauss-Markov processes. Huang and Chiang (2008) proposed an intelligent scheme to integrate INS/GPS navigation system based on constructive neural network (CNN). A reliable in-motion alignment algorithm for low-cost strap-down inertial navigation systems has been presented in Ali and Ushaq (2009). Noureldin et al. (2011) used artificial neural networks to approximate nonlinear terms of the integration filter in INS/GNSS systems. Aiming to enhance positioning accuracy of the INS/GNSS system during GNSS outages, Chen et al. (2013) proposed a model combining strong tracking Kalman filter (STKF) and wavelet neural network (WNN) algorithms for INS error compensation. Musavi and Keighobadi (2015) presented an adaptive neuro-fuzzy observer to improve the performance of INS/GNSS integrated positioning systems. Magnetic calibration of strap-down magnetometers for the INS heading angle correction has been presented in Milanchian et al. (2015). According to covariance matching techniques, Meng et al. (2016) developed an adaptive unscented Kalman filter (UKF) for the integration algorithm of INS/GNSS system. Despite of valuable research published, there are crucial factors that restrict the practical application of some research carried out in the field of integrated INS/GNSS navigation systems. For example, the integration scheme should be mathematically non-singular, computationally efficient, and real-time in implementation.

Integration mechanization and state estimation algorithms are two essential steps for the fusion of INS and the GNSS data. In most of the previous research, attention was focused on the state estimation algorithms and considerable enhancement was achieved. We focused on the integration scheme of the INS/GNSS system, especially in the case of using MEMS-grade IMU in the INS. Two different mechanizations, called indirect centralized (IC) and direct decentralized (DD) integration, are designed and implemented. In case of IC integration, a linearized INS error model is incorporated in the estimation algorithm. Moreover, the estimation process is performed in a central filter. In the DD integration, basic INS nonlinear dynamics are used in the estimation algorithm. A new technique is used in the estimation process of the DD integration scheme. Aiming at removing the estimation error in position and velocity components on orientation (attitude and heading angles) estimation, the orientation filter is separated from the position/velocity filter. In the IC integration scheme, the orientation states are corrected based on the misalignment matrix estimated during the navigation process. On the other hand, in the DD integration scheme, gravity attitude angles computed from outputs of accelerometers are used as measurements in the state estimation filter. Assessment of each procedure, IC and DD integration should be conducted in field tests under various dynamical maneuverings. Furthermore, it is very important to compare them in terms of reliability and accuracy, especially in the case of GNSS signal blockage. The main contributions of this research can be summarized as follows:

- Design of IC integration scheme for low-cost INS/GNSS navigation system.
- Design of DD integration scheme for low-cost INS/GNSS navigation system.
- Enhancing the navigation accuracy of INS/GNSS system during GNSS outages based on auxiliary velocity-update approach.
- Experimental evaluation of IC and DD integration schemes in different dynamical maneuverings.

Experimental evaluation of the proposed approaches is conducted via field tests implemented on land and airborne vehicles. An ADIS-16407 IMU is used as a complete inertial system which consists of three-axis MEMS accelerometer and gyroscope. A Garmin-35 receiver provides the GNSS position and velocity measurements.

General INS equations

General inertial navigation equations contain two dynamical systems including basic nonlinear INS dynamics and linearized INS error dynamics, as described in the following sections. Inertial frame (i-frame), earth frame (e-frame) navigation frame (n-frame) and body frame (b-frame) are the main reference frames used here.

Basic INS dynamics

Basic INS equations acquire linear and angular measurements of three-axis accelerometer and gyroscope in the b-frame and return final orientation, position and velocity components in the n-frame. The INS system of equations in the n-frame is represented as follows (Nourmohammadi and Keighobadi 2017):

$$\dot{L} = \frac{v_N}{R_N + h}, \quad \dot{l} = \frac{v_E}{(R_E + h)\cos L}, \quad \dot{h} = -v_D, \tag{1}$$

$$\begin{aligned}
\dot{v}_N &= f_N - 2\omega_e v_E \sin L + \frac{v_N v_D}{R_N + h} - \frac{v_E^2 \tan L}{R_E + h} \\
\dot{v}_E &= f_E + 2\omega_e (v_N \sin L + v_D \cos L) + \frac{v_E \left(v_D + v_N \sin L\right)}{R_E + h} \\
\dot{v}_D &= f_D - 2\omega_e v_E \cos L - \frac{v_E^2}{R_E + h} + \frac{v_N^2}{R_N + h} + g,
\end{aligned} \tag{2}$$

$$\begin{aligned}\dot{\varphi} &= \left(\omega_y \sin\varphi + \omega_z \cos\varphi\right)\tan\theta + \omega_x \\ \dot{\theta} &= \omega_y \cos\varphi - \omega_z \sin\varphi \\ \dot{\psi} &= \left(\omega_y \sin\varphi + \omega_z \cos\varphi\right)\sec\theta,\end{aligned} \tag{3}$$

where L, l, and h are geographical latitude, longitude, and height; $\mathbf{v}^n = \begin{bmatrix} v_N & v_E & v_D \end{bmatrix}^T$ is the velocity vector in the n-frame; $\mathbf{f}^n = \begin{bmatrix} f_N & f_E & f_D \end{bmatrix}^T$ is the specific force vector expressed in the n-frame; R_N and R_E are earth meridian and transverse radii of curvature; ω_e and g are earth angular rate and gravity; the orientation yaw-pitch-roll angles shown as ψ, θ, and φ specify rotation components about z, y, and x body axes, respectively. Moreover, in the Euler angles dynamics of (3), ω_x, ω_y, and ω_z are the components of $\boldsymbol{\omega}^b_{nb}$, as the rotation rate of the b-frame with respect to the n-frame expressed in the b-frame. $\boldsymbol{\omega}^b_{nb}$ is obtained from gyroscope rate vector, $\boldsymbol{\omega}^b_{ib}$ as follows (Titterton and Weston 2004):

$$\boldsymbol{\omega}^b_{nb} = [\omega_x \ \omega_y \ \omega_z]^T = \boldsymbol{\omega}^b_{ib} - \mathbf{C}^b_n[\boldsymbol{\omega}^n_{ie} + \boldsymbol{\omega}^n_{en}], \tag{4}$$

where $\boldsymbol{\omega}^n_{ie}$ stands for earth rate vector projected in the n-frame and $\boldsymbol{\omega}^n_{en}$ is the rotation rate of the n-frame with respect to the e-frame. $\mathbf{C}^n_b$ is direction cosine matrix (DCM) between the b-frame and the n-frame (Keighobadi 2011),

$$\mathbf{C}^n_b = \begin{bmatrix} C\theta\, C\psi & -C\varphi\, S\psi + S\varphi\, S\theta\, C\psi & S\varphi\, S\psi + C\varphi\, S\theta\, C\psi \\ C\theta\, S\psi & C\varphi\, C\psi + S\varphi\, S\theta\, S\psi & -S\varphi\, C\psi + C\varphi\, S\theta\, S\psi \\ -S\theta & S\varphi\, C\theta & C\varphi\, C\theta \end{bmatrix}, \tag{5}$$

where S and C stand for sine and cosine functions, respectively. Using (1)–(5), the navigation data is continuously updated after receiving the IMU measurements. However, owing to large error of MEMS-grade IMU, the navigation accuracy of the stand-alone INS degrades over time, quickly.

INS error dynamics

In the INS error dynamics, the state vector consists of fifteen states, including three misalignment errors ($\delta\alpha$, $\delta\beta$, $\delta\gamma$), three velocity errors (δv_N, δv_E, δv_D), three position errors (δL, δl, δh), accelerometer biases in the n-frame (B_N, B_E, B_D), and gyroscope drifts in the n-frame (D_N, D_E, D_D). The standard form of the INS error dynamics are expressed based on the following equations (Stancic and Graovac 2010),

$$\begin{aligned}
\delta\dot{\alpha} &= -\left(\omega_e \sin L + \frac{v_E \tan L}{R_E + h}\right)\delta\beta + \frac{v_N}{R_N + h}\delta\gamma + \frac{1}{R_E + h}\delta v_E - \omega_e \sin L\, \delta L - \frac{v_E}{(R_E + h)^2}\delta h - D_N \\
\delta\dot{\beta} &= \left(\omega_e \sin L + \frac{v_E \tan L}{R_E + h}\right)\delta\alpha + \left(\omega_e \cos L + \frac{v_E}{R_E + h}\right)\delta\gamma - \frac{1}{R_N + h}\delta v_N + \frac{v_N}{(R_N + h)^2}\delta h - D_E \\
\delta\dot{\gamma} &= -\frac{v_N}{R_N + h}\delta\alpha - \left(\omega_e \cos L + \frac{v_E}{R_E + h}\right)\delta\beta - \frac{\tan L}{R_E + h}\delta v_E - \left(\omega_e \cos L + \frac{v_E}{(R_E + h)\cos^2 L}\right)\delta L + \frac{v_E \tan L}{(R_E + h)^2}\delta h - D_D,
\end{aligned} \tag{6}$$

$$\begin{aligned}
\delta\dot{v}_N = &-f_D\,\delta\beta + f_E\,\delta\gamma + \frac{v_D}{R_N + h}\delta v_N - 2\sin L\left(\omega_e + \frac{v_E}{(R_E + h)\cos L}\right)\delta v_E + \frac{v_N}{R_N + h}\delta v_D \\
&- \left(2\omega_e v_E \cos L + \frac{v_E^2}{(R_E + h)\cos^2 L}\right)\delta L + \left(\frac{v_E^2 \tan L}{(R_E + h)^2} - \frac{v_N v_D}{(R_N + h)^2}\right)\delta h + B_N,
\end{aligned} \tag{7.1}$$

$$\begin{aligned}
\delta\dot{v}_E = &\, f_D\,\delta\alpha - f_N\,\delta\gamma + \left(2\omega_e \sin L + \frac{v_E \tan L}{R_E + h}\right)\delta v_N + \left(\frac{v_D + v_N \tan L}{R_E + h}\right)\delta v_E + \left(2\omega_e \cos L + \frac{v_E}{R_E + h}\right)\delta v_D \\
&+ \left(2\omega_e\left(v_N \cos L - v_D \sin L\right) + \frac{v_N v_E}{(R_E + h)\cos^2 L}\right)\delta L - \left(\frac{v_E(v_D + v_N \tan L)}{(R_E + h)^2}\right)\delta h + B_E,
\end{aligned} \tag{7.2}$$

$$\begin{aligned}
\delta\dot{v}_D = &-f_E\,\delta\alpha + f_N\,\delta\beta - \frac{2v_N}{R_N + h}\delta v_N - 2\left(\omega_e \cos L + \frac{v_E}{R_E + h}\right)\delta v_E + 2\omega_e v_E \sin L\, \delta L \\
&+ \left(\frac{v_E^2}{(R_E + h)^2} + \frac{v_N^2}{(R_N + h)^2} - \frac{2g}{R + h}\right)\delta h + B_D,
\end{aligned} \tag{7.3}$$

$$\begin{aligned}
\delta\dot{L} &= \frac{-v_N}{(R_N+h)^2}\delta h + \frac{1}{R_N+h}\delta v_N \\
\delta\dot{l} &= \frac{v_E \sin L}{(R_E+h)\cos^2 L}\delta L + \frac{-v_E}{(R_E+h)^2\cos L}\delta h + \frac{1}{(R_E+h)\cos L}\delta v_E \\
\delta\dot{h} &= -\delta v_D,
\end{aligned} \tag{8}$$

$$\begin{aligned}
\dot{D}_i &= -\beta D_i + \sigma\sqrt{2\beta}\, w(t), \quad i = N, E, D \\
\dot{B}_i &= 0, \quad i = N, E, D
\end{aligned} \tag{9}$$

where the symbol δ represents the perturbation from the true value. For example, δL is defined as $\hat{L} - L$ in which, the element with (^) is the estimated quantity and that without (^) is the true quantity. In the IMU error dynamics of (9), it is assumed that the gyroscope drifts can be modeled by first order Gauss–Markov process and the accelerometer biases by constant values. In (9), the σ and β stand for variance and correlation coefficient of the Gauss–Markov process, respectively, and $w(t)$ denotes zero-mean Gaussian white noise.

The estimated rotation matrix, $\hat{\mathbf{C}}_n^b$ can be written in terms of the true rotation matrix and the misalignment errors. Based on Poisson equation it can be formulated as (Rogers 2003),

$$\hat{\mathbf{C}}_b^n = [\mathbf{I} - \mathbf{E}]\mathbf{C}_b^n, \tag{10}$$

where $\mathbf{I}$ is identity matrix and $\mathbf{E}$ shows skew-symmetric form of the misalignment vector,

$$\mathbf{E} = \begin{bmatrix} 0 & -\delta\gamma & \delta\beta \\ \delta\gamma & 0 & -\delta\alpha \\ -\delta\beta & \delta\alpha & 0 \end{bmatrix}. \tag{11}$$

The estimated orientation angles are corrected using the misalignment components in (10).

Integrated INS/GNSS system

INS and GNSS systems are complementary in many aspects. For example, INS provides continuous data at high update rate, while GNSS suffers from signal blockage and low updating rate. On the other hand, GNSS error is more stable and effectively time-invariant, while INS suffers from time-increasing navigation error in long-term applications. Additionally, INS systems provide complete navigation states, but a single GNSS receiver cannot supply orientation angles. The above-mentioned descriptions motivate developing an integrated INS/GNSS navigation system. The INS is integrated with GNSS to enhance the overall navigation accuracy and reliability. In the following sections, two applied configurations are presented for the integration of a GNSS receiver with the INS system.

IC integration scheme

IC integration scheme is developed based on the use of INS error model in the estimation process of the integrated INS/GNSS system. Indirect integration implies that the navigation information, including position, velocity, and orientation are not directly estimated in the corresponding estimation filter. The INS error states are estimated in the estimation filter and then the INS navigation states are corrected based on the estimated error states. Centralized integration implies that the estimation process is accomplished in a single central filter. The block diagram of Fig. 1 shows the configuration of the proposed IC integrated INS/GNSS.

The proposed IC integration scheme is accomplished in accordance with the following procedure:

1. Basic INS dynamics are the mechanization equations expressed in (1)–(3). The accelerometer and the gyroscope outputs are received and then the INS states, including position, velocity, and orientation components are computed in the INS dynamics.
2. INS error dynamics, expressed in (6)–(9), are used as the dynamics system of state estimation algorithm. The INS error states are constituted as the following vector:

$$\mathbf{x} = [\delta\alpha \;\; \delta\beta \;\; \delta\gamma \;\; \delta v_N \;\; \delta v_E \;\; \delta v_D \;\; \delta L \;\; \delta l \;\; \delta h \;\; D_N \;\; D_E \;\; D_D \;\; B_N \;\; B_E \;\; B_D]^T \tag{12}$$

3. The measurement vector of the state estimation algorithm is constituted from GNSS position, velocity, and heading data as follows:

$$\mathbf{z} = \begin{bmatrix} \boldsymbol{v}^{INS} - \boldsymbol{v}^{G} \\ \boldsymbol{r}^{INS} - \boldsymbol{r}^{G} \\ \psi^{INS} - \psi^{G} \end{bmatrix} \tag{13}$$

where $\boldsymbol{v} = [v_N \;\; v_E \;\; v_D]^T$ and $\boldsymbol{r} = [L \;\; l \;\; h]^T$.

4. Kalman filter is used as the estimation algorithm of the proposed IC integration scheme. Misalignment errors, velocity errors, position errors, and IMU errors are estimated as the state variables.
5. Accelerometer biases and gyroscope drifts are compensated as follows:

$$\begin{aligned}
\boldsymbol{\omega} &= \hat{\boldsymbol{\omega}} - \boldsymbol{D} \\
\boldsymbol{f} &= \hat{\boldsymbol{f}} - \boldsymbol{B}
\end{aligned} \tag{14}$$

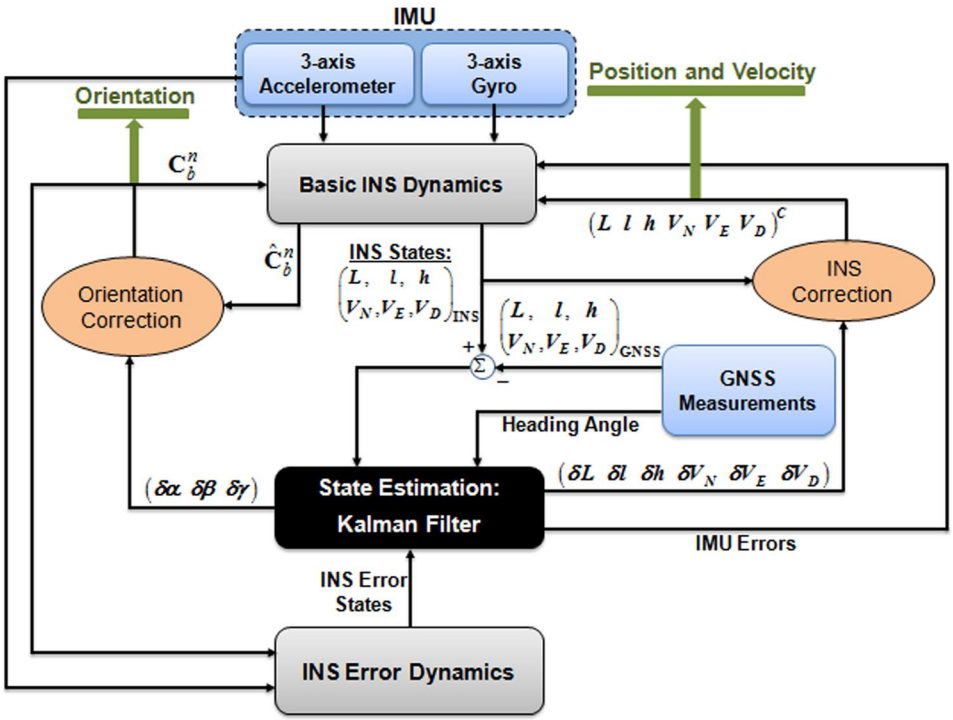

Fig. 1 IC integration scheme for INS/GNSS system

where $\boldsymbol{\omega}$ and $\hat{\boldsymbol{\omega}}$ stand for the corrected and erroneous gyroscope rates, respectively. Similarly, $\boldsymbol{f}$ and $\hat{\boldsymbol{f}}$ stand for the corrected and erroneous accelerometer specific forces, respectively. The corrected values of gyroscope rates and specific forces are fed into the INS dynamics.

6. Based on (10) and (11), the DCM matrix is corrected by use of the estimated misalignment errors. Consequently, the orientation yaw-pitch-roll angles are computed from the corrected DCM matrix.
7. The INS position and velocity components are corrected as follows:

$$\begin{aligned} L^C &= L^{INS} - \delta L, \quad l^C = l^{INS} - \delta l, \quad h^C = h^{INS} - \delta h \\ v_N^C &= v_N^{INS} - \delta v_N, \quad v_E^C = v_E^{INS} - \delta v_E, \quad v_D^C = v_D^{INS} - \delta v_D \end{aligned} \tag{15}$$

8. The corrected values of the orientation, position, and velocity components are fed back into the basic INS dynamics.

We now describe the estimation filter of the proposed IC integration scheme in more detail. Since the dynamics system is linear, the standard Kalman filter is applied as the estimation filter of the IC integration scheme. The Kalman filter is implemented in two steps so-called as time-update and measurement-update (Simon 2006). In time-update the predicted values of the error covariance, $\boldsymbol{P}_k^-$ and the state vector, $\hat{\mathbf{x}}_k^-$ are computed as follows:

$$\mathbf{P}_k^- = \boldsymbol{\Phi}_{k-1}\mathbf{P}_{k-1}\boldsymbol{\Phi}_{k-1}^T + \mathbf{Q}_{k-1} \tag{16.1}$$

$$\hat{\mathbf{x}}_k^- = \boldsymbol{\Phi}_{k-1}\hat{\mathbf{x}}_{k-1} \tag{16.2}$$

where $\boldsymbol{\Phi}_{k-1}$ stands for the state-transition matrix computed from the dynamics system of (6)–(9). The covariance matrix of system noise has been characterized by $\mathbf{Q}_{k-1}$. In measurement-update, the Kalman gain, $\boldsymbol{K}_k$ is calculated first, and then the state vector and the error covariance matrix are updated as follows:

$$\mathbf{K}_k = \mathbf{P}_k^-\mathbf{H}_k^T\left(\mathbf{H}_k\mathbf{P}_k^-\mathbf{H}_k^T + \mathbf{R}_k\right)^{-1} \tag{17.1}$$

$$\hat{\mathbf{x}}_k = \hat{\mathbf{x}}_k^- + \mathbf{K}_k\left[\mathbf{z}_k - \mathbf{H}_k\,\hat{\mathbf{x}}_k^-\right] \tag{17.2}$$

$$\mathbf{P}_k = \left(\mathbf{I} - \mathbf{K}_k\mathbf{H}_k\right)\mathbf{P}_k^- \tag{17.3}$$

where $\mathbf{R}_k$ denotes the covariance matrix of measurement noise and the observation matrix $\mathbf{H}_k$ is constituted as follows:

$$\mathbf{H} = \begin{bmatrix} \mathbf{0}_{3\times3} & \boldsymbol{I}_{3\times3} & \mathbf{0}_{3\times3} & \mathbf{0}_{3\times3} & \mathbf{0}_{3\times3} \\ \mathbf{0}_{3\times3} & \mathbf{0}_{3\times3} & \boldsymbol{I}_{3\times3} & \mathbf{0}_{3\times3} & \mathbf{0}_{3\times3} \\ 0\ \ 0\ \ -1 & \mathbf{0}_{1\times3} & 0_{1\times3} & \mathbf{0}_{1\times3} & \mathbf{0}_{1\times3} \end{bmatrix} \tag{18}$$

The above observation matrix has been constituted based on the state vector of (12) and the measurement vector of (13).

There are two underlying concepts behind the integration scheme of the proposed IC integrated INS/GNSS system.

As to the first concept, the INS outputs can be incorporated with the estimated error states based on two strategies

including feed-forward method and feedback method. In the feed-forward method, the INS system operates as a black box which is unaware of the results of estimation filter. Conversely, in the feedback method, the corrected navigation data are fed back into the INS system in every time step. The main drawback of the feed-forward method is that the INS error increases unboundedly. As a matter of fact, since only small errors are permitted due to the linearization process, the unbounded INS error causes a substantial problem to the linear filter of the IC integration scheme. Therefore, the feedback method is more efficient, particularly in low-cost INSs. According to above explanations, feedback strategy has been used in the proposed IC integration scheme, as shown in the block diagram of Fig. 1.

As to the second concept, in every time step the estimated error states are fed back into the INS system. After each feedback, the INS outputs are corrected and the error state vector should be set to zero. Since feedback is carried out whenever measurements are received, the state prediction (16.2) in time-update does not need to be run at all. Consequently, (17.2) reduces to:

$$\hat{\mathbf{x}}_k = \mathbf{K}_k \, \mathbf{z}_k \tag{19}$$

This enhances the reliability and numerical stability of the estimation filter in the proposed IC integrated INS/GNSS system.

DD integration scheme

Direct integration indicates that the general INS nonlinear dynamics are used in the estimation process. Therefore, the navigation information, including position, velocity, and orientation are directly estimated in the corresponding estimation filter. Decentralized integration indicates that the estimation process is accomplished in two cascade filters. In other words, the orientation estimation is separated from the position and velocity estimation filter. The block diagram of Fig. 2 shows the configuration of the proposed DD integrated INS/GNSS system. The proposed DD integration scheme is accomplished in accordance with the following procedure.

1. Dynamics system of the orientation filter uses a six-state vector including roll-pitch-yaw angles and gyroscope drift components along body x–y–z-axes. Adding gyro-

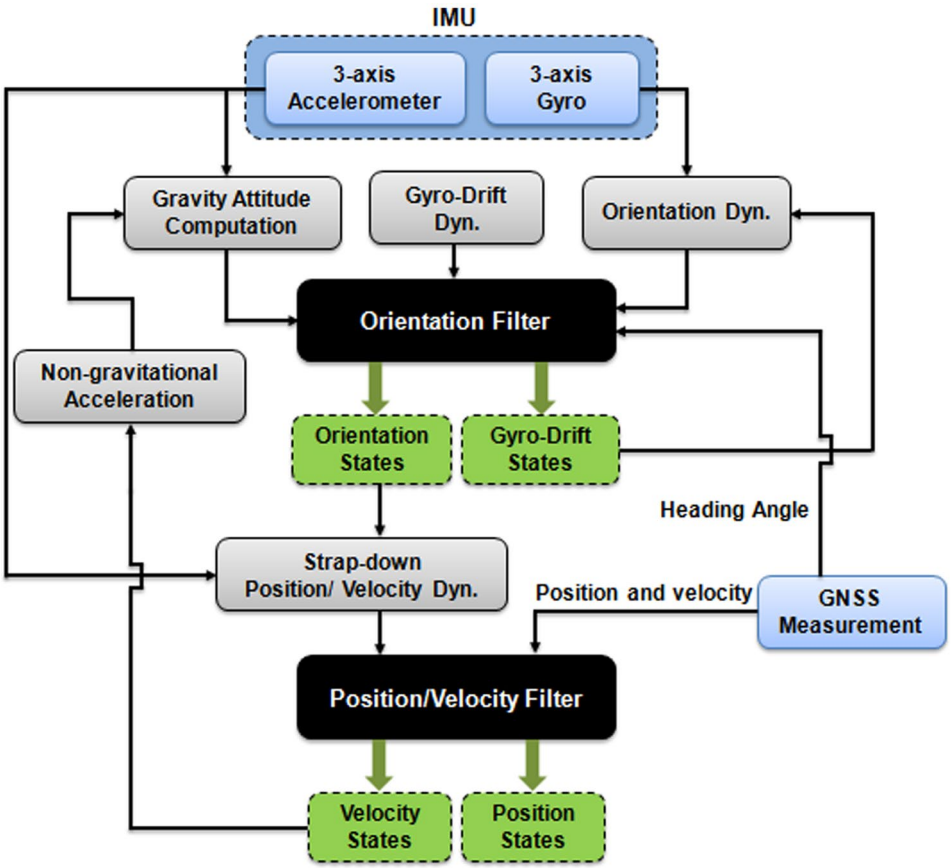

Fig. 2 DD integration scheme for INS/GNSS system

scope drift components to (3) leads to the following dynamics,

$$\begin{aligned}\dot{\varphi} &= \big((\omega_y - D_y)\sin\varphi + (\omega_z - D_z)\cos\varphi\big)\tan\theta + \omega_x - D_x\\ \dot{\theta} &= (\omega_y - D_y)\cos\varphi - (\omega_z - D_z)\sin\varphi\\ \dot{\psi} &= \big((\omega_y - D_y)\sin\varphi + (\omega_z - D_z)\cos\varphi\big)\sec\theta,\end{aligned} \tag{20.1}$$

$$\dot{D}_i = -\beta D_i + \sigma\sqrt{2\beta}\, w(t), \qquad i = x, y, z \tag{20.2}$$

2. Accelerometer-sensed gravity in the b-frame is matched with the reference gravity in the n-frame as follows (Nourmohammadi and Keighobadi 2018),

$$\frac{1}{norm(\boldsymbol{f}^b)}\begin{bmatrix} f_x^b \\ f_y^b \\ f_z^b \end{bmatrix} = [\boldsymbol{C}_n^b]\begin{bmatrix} 0 \\ 0 \\ -1 \end{bmatrix} \tag{21}$$

3. Non-gravitational acceleration terms are canceled in the accelerometer outputs.

$$(f_x^b)_g = f_x^b - \text{sign}\big(\text{norm}(\boldsymbol{f}^b) - \text{norm}(\boldsymbol{f}_0^b)\big)\text{norm}(\dot{\boldsymbol{v}}^n) \tag{22}$$

where $\boldsymbol{f}_0^b$ stands for the accelerometer output vector in a stationary mode. In (22), we used the fact that the non-gravitational acceleration of the host (under navigation) vehicle is mainly generated along the body x-axis known as longitudinal axis.

4. The gravity attitude angles are obtained as follows:

$$\begin{aligned}\varphi^{\text{acc}} &= a\tan 2\Big(-f_y^b,\ -f_z^b\Big)\\ \theta^{\text{acc}} &= a\sin\left(\frac{(f_x^b)_g}{\text{norm}(\boldsymbol{f}_0^b)}\right)\end{aligned} \tag{23}$$

where φ^{acc} and θ^{acc} are the gravity matching-based roll and pitch angles, respectively.

5. For the orientation filter, the measurement vector is constructed as follows:

$$\mathbf{z}_1 = \begin{bmatrix} \varphi^{acc} & \theta^{acc} & \psi^G \end{bmatrix}^T \tag{24}$$

where ψ^G is the GNSS heading angle.

6. The nonlinear Kalman filter is carried out on the dynamics system of (20) with the measurement vector of (24). So, the orientation states and the gyroscope drifts are estimated.
7. The estimated orientation angles are fed into the position and velocity dynamics of (1) and (2).
8. For the position and velocity filter, the measurement vector is constructed from GNSS position and velocity data as follows:

$$\mathbf{z}_2 = \begin{bmatrix} L^G & l^G & h^G & v_N^G & v_E^G & v_D^G \end{bmatrix}^T \tag{25}$$

where, for example, L^G stands for the GNSS latitude.

9. The nonlinear Kalman filter is carried out on the dynamics system of (1) and (2) with the measurement vector of (25). So, the position and velocity states are estimated.

As the main advantage, in the DD integration scheme the linearized INS error model is replaced by the basic INS nonlinear dynamics. Therefore, the linearization error does not affect the estimation accuracy of the integrated navigation system.

We now describe the estimation filter used in the proposed DD integration scheme in more detail. Owing to the nonlinear dynamics system of the DD integrated INS/GNSS system, the nonlinear Kalman filter should be applied. EKF is probably the most widely used estimation algorithm for nonlinear systems. However, it is not an optimal estimator, in general. EKF suffers from some drawbacks which mainly arise from its linearization-based structure. For example, in the case of bad initialization, the filter may quickly diverge. Moreover, for non-differentiable nonlinear systems with high nonlinearity, large error occurs in mean and covariance of state estimation in EKF, owing to its linearization. Unscented Kalman filter (UKF) and cubature Kalman filter (CKF) are two other nonlinear Kalman filter that show promise as an improvement over EKF. In the UKF, a set of carefully chosen sigma-points are used to carry out an unscented transformation based on Gaussian distribution. Accordingly, the mean and covariance values of the posterior estimation are captured. By reducing Bayesian filter to a problem of computing multi-dimensional Gaussian-weighted integrals, a new filter CKF has been introduced. The CKF uses a nonlinear transformation based on the radial-spherical cubature rule. Unlike the UKF, the CKF does not apply the central sigma point which commonly has negative weight in high-dimensional systems. Moreover, there is no tuning parameter in the CKF. In general, the CKF improves the numerical stability characteristic in high-dimensional estimation problem over the UKF (Chang et al. 2013).

Taking into account the above discussion, we use the CKF as the estimation algorithm in the proposed DD integrated INS/GNSS system. The CKF is performed in accordance with the following procedure (Arasaratnam and Haykin 2009):

Step-1: Initialization

The state vector and error covariance matrix are initialized.

$$\begin{aligned}\hat{\mathbf{x}}_{0|0} &= \mathbb{E}(\mathbf{x}_{0|0})\\ \mathbf{P}_{0|0} &= \mathbb{E}[(\mathbf{x}_{0|0} - \hat{\mathbf{x}}_{0|0})(\mathbf{x}_{0|0} - \hat{\mathbf{x}}_{0|0})^T].\end{aligned} \tag{26}$$

Step-2: Time update

Square-root value of the covariance matrix is calculated in accordance with $\mathbf{S}_{k-1|k-1}\mathbf{S}_{k-1|k-1}^{T} = \mathbf{P}_{k-1|k-1}$. The cubature points are computed for $i = 1, 2, \ldots, 2n$.

$$\mathbf{X}_{i,k-1|k-1} = \mathbf{S}_{k-1|k-1}\,\boldsymbol{\zeta}_i + \hat{\mathbf{x}}_{k-1|k-1}, \tag{27}$$

where $\boldsymbol{\zeta}_i$ is ith column of matrix $\sqrt{\mathrm{n}}\left[\,\mathbf{I}_{\mathrm{n}\times\mathrm{n}}\ -\mathbf{I}_{\mathrm{n}\times\mathrm{n}}\,\right]$. Then the points are propagated based on the state dynamics model,

$$\mathbf{X}_{i,k|k-1}^{*} = \mathbf{f}\left(\mathbf{X}_{i,k-1|k-1}\right), \tag{28}$$

where $\mathbf{f}(\cdot)$ is a nonlinear vector characterizing the dynamics system. It should be noticed that $\mathbf{f}(\cdot)$ is the discrete-time form of the associated dynamics system playing the role of state transition matrix in the linear system.

The mean and covariance of the predicted state are computed as follows:

$$\hat{\mathbf{x}}_{k|k-1} = \frac{1}{2n}\sum_{i=1}^{2n}\mathbf{X}_{i,k|k-1}^{*}, \tag{29}$$

$$\mathbf{P}_{k|k-1} = \frac{1}{2n}\sum_{i=1}^{2n}\mathbf{X}_{i,k|k-1}^{*}\,\mathbf{X}_{i,k|k-1}^{*T} - \hat{\mathbf{x}}_{k|k-1}\,\hat{\mathbf{x}}_{k|k-1}^{T} + \mathbf{Q}_{k-1} \tag{30}$$

Step-3: Measurement update

Using time-updated state vector and covariance matrix, new cubature points are computed as,

$$\mathbf{X}_{i,k|k-1} = \mathbf{S}_{k|k-1}\,\boldsymbol{\zeta}_i + \hat{\mathbf{x}}_{k|k-1}. \tag{31}$$

The points are propagated based on the measurement equation,

$$\mathbf{Y}_{i,k|k-1} = \mathbf{h}\left(\mathbf{X}_{i,k|k-1}\right). \tag{32}$$

where $\mathbf{h}(\cdot)$ is a nonlinear vector characterizing the ideal noiseless relationship between the state and measurement vector. Then, the predicted measurement vector is computed,

$$\hat{\mathbf{y}}_{k|k-1} = \frac{1}{2n}\sum_{i=1}^{2n}\mathbf{Y}_{i,k|k-1} \tag{33}$$

The cross-covariance and innovation covariance matrices are obtained as follows,

$$\mathbf{P}_{xy,k|k-1} = \frac{1}{2n}\sum_{i=1}^{2n}\mathbf{X}_{i,k|k-1}\,\mathbf{Y}_{i,k|k-1}^{T} - \hat{\mathbf{x}}_{k|k-1}\,\hat{\mathbf{y}}_{k|k-1}^{T} \tag{34}$$

$$\mathbf{P}_{y,k|k-1} = \frac{1}{2n}\sum_{i=1}^{2n}\mathbf{Y}_{i,k|k-1}\,\mathbf{Y}_{i,k|k-1}^{T} - \hat{\mathbf{y}}_{k|k-1}\,\hat{\mathbf{y}}_{k|k-1}^{T} + \mathbf{R}_k \tag{35}$$

Kalman gain is computed as,

$$\mathbf{K}_k = \mathbf{P}_{xy,k|k-1}\,\mathbf{P}_{y,k|k-1}^{-1} \tag{36}$$

Finally, the measurement-updated state vector and its covariance matrix are obtained,

$$\hat{\mathbf{x}}_{k|k} = \hat{\mathbf{x}}_{k|k-1} + \mathbf{K}_k(\mathbf{y}_k - \hat{\mathbf{y}}_{k|k-1}) \tag{37}$$

$$\mathbf{P}_{k|k} = \mathbf{P}_{k|k-1} - \mathbf{K}_k\,\mathbf{P}_{y,k|k-1}\,\mathbf{K}_k^{T} \tag{38}$$

The CKF does not use Jacobian matrices in the nonlinear filtering problem in which the large linearization errors may lead to the failure of the filter. Taking into account the limited accuracy of the MEMS-grade IMU in the low-cost INS/GNSS system, the CKF algorithm results in improved numerical stability and accuracy relative to the traditional EKF.

In case of GNSS outages

One of the main challenges in the integrated INS/GNSS system is the navigation accuracy and reliability during abrupt signal blockage of GNSS system. During GNSS outages, the INS correction and error compensation are stopped until the GNSS signals are reacquired. Due to large errors and uncertainties of low-quality MEMS-grade IMU, it is obvious that the INS accuracy and performance will quickly degrade in the absence of GNSS signals. Therefore, it is very important to develop an approach for accuracy enhancement of the INS/GNSS system during GNSS outages, especially if an MEMS-grade IMU is used in the INS system. In this section, based on vehicle's motion attributes and constraints, an approach is proposed to prevent INS error accumulation during GNSS outages.

Using the fact that the non-gravitational acceleration of the host vehicle is mainly generated along its longitudinal axis, auxiliary velocity-updates (AVUs) can be provided based on non-holonomic constraint (NHC) and axial-derived velocity (ADV). NHC is a 2D non-holonomic constraint in which the lateral and vertical components of the vehicle velocity are assumed to be close to zero. ADV is a 1D forward velocity that can be considered in the vehicle velocity update. ADV is supplied by any type of axial speed sensor such as odometer. Therefore, the aforementioned AVUs can be expressed as follows:

$$\begin{aligned} v_x^b &= v_{\text{axial}} \\ v_y^b &\approx 0 \\ v_z^b &\approx 0 \end{aligned} \tag{39}$$

where v_x^b, v_y^b, and v_z^b specify the x–y–z components of the vehicle velocity in the b-frame and v_{axial} is the forward velocity measured by axial speed sensor. Although AVUs are

usually used in periods of GNSS outages, it could enhance the integration performance in a weak signal and multipath environment.

The auxiliary velocity is transformed into the n-frame. Accordingly, the virtual velocity measurements are constructed,

$$\begin{bmatrix} v_N^{\text{aid}} \\ v_E^{\text{aid}} \\ v_D^{\text{aid}} \end{bmatrix} = \left[\boldsymbol{C}_b^n\right] \begin{bmatrix} v_{\text{axial}} \\ 0 \\ 0 \end{bmatrix} \tag{40}$$

Equation (40) can be rewritten as follows:

$$\begin{aligned} v_N^{\text{aid}} &= v_{\text{axial}} \cos\theta \cos\psi \\ v_E^{\text{aid}} &= v_{\text{axial}} \cos\theta \sin\psi \\ v_D^{\text{aid}} &= -v_{\text{axial}} \sin\theta \end{aligned} \tag{41}$$

Then, the virtual position measurements are obtained using the INS position dynamics of (1).

$$\begin{aligned} L^{\text{aid}}(k) &= \frac{v_N^{\text{aid}}(k)\Delta t}{R_N + h^{\text{aid}}(k-1)} + L^{\text{aid}}(k-1) \\ l^{\text{aid}}(k) &= \frac{v_E^{\text{aid}}(k)\Delta t}{\left(R_E + h^{\text{aid}}(k-1)\right)\cos L^{\text{aid}}(k-1)} + l^{\text{aid}}(k-1) \\ h^{\text{aid}}(k) &= -v_D^{\text{aid}}(k)\Delta t + h^{\text{aid}}(k-1) \end{aligned} \tag{42}$$

where Δt stands for the time step of measurement update. The above-mentioned virtual measurements are used in the estimation filter of the INS/GNSS system whenever the GNSS signals are lost. Accordingly, in GNSS gaps, the measurement vector of the IC integration scheme is constructed as follows:

$$\mathbf{z} = \begin{bmatrix} \boldsymbol{v}^{\text{INS}} - \boldsymbol{v}^{\text{aid}} \\ \boldsymbol{r}^{\text{INS}} - \boldsymbol{r}^{\text{aid}} \\ \psi^{\text{INS}} - \psi \end{bmatrix} \tag{43}$$

As shown in (43), in case of GNSS gaps, the measurement value of the heading angle is set to the estimated heading angle. Furthermore, the estimated drift of the z-gyroscope is not reliable at all. Accordingly, the drift estimation of the z-gyroscope should be stopped until the GNSS signals are reacquired. During these periods, the filter operates with the last drift estimated just before the GNSS signal blockage. By implementing the proposed procedure, the estimation error of the heading angle will be noticeably controlled.

Similarly, the measurement vectors of the orientation filter and the position and velocity filter in the DD integration scheme are constructed as follows:

$$\mathbf{z}_1 = \begin{bmatrix} \varphi^{acc} & \theta^{acc} & \psi \end{bmatrix}^T \tag{44}$$

$$\mathbf{z}_2 = \begin{bmatrix} L^{aid} & l^{aid} & h^{aid} & v_N^{aid} & v_E^{aid} & v_D^{aid} \end{bmatrix}^T \tag{45}$$

The same procedure is adopted to bound the estimation error of the heading angle during the GNSS outages, as explained above for the IC integration scheme.

Experimental results and discussion

Several land and flight tests have been arranged for experimental evaluation of the proposed IC and DD integrated INS/GNSS systems. An ADIS-16407 IMU is used as a complete inertial system consisting three-axis MEMS accelerometer and gyroscope. The main physical and operating characteristics of the inertial sensors in the ADIS-16407 IMU are summarized in Table 1.

The sensitive axes of the IMU are fixed along the body axes of the vehicle. The Garmin-35 receiver provides the GNSS position and velocity measurements. Attitude estimation accuracy of the proposed IC and DD integration schemes is assessed in comparison with highly accurate Vitans navigation system. The main equipment used in the field tests are shown in Fig. 3.

Data acquisition of the inertial sensors is made at the sampling frequency of 50 Hz and the GNSS updating frequency is 1 Hz. Two types of field tests have been arranged to verify the proposed INS/GNSS systems. The first one is implemented on an airborne vehicle and the second one on a land vehicle. Figure 4 represents the vehicle trajectory during the flight test.

As shown in Fig. 4, the flight test has been executed for approximately 1600s along a high-maneuvered trajectory. The performance of the proposed IC and DD integrated INS/GNSS systems in orientation is shown in Fig. 5. The attitude angles obtained by the highly accurate Vitans system are used to evaluate the attitude estimation accuracy of the proposed algorithms. The estimated heading angle is evaluated in comparison to the GNSS heading angle. Figure 6 shows the estimated gyroscope drift components in the b-frame.

Table 1 Main characteristics of the inertial sensor in ADIS-16407

Parameter	Gyroscope	Accelerometer
In-run bias stability (1σ)	0.007°/s	0.2 mg
Random walk (1σ)	$1.9°/\sqrt{\text{h}}$	$0.2\ \text{m/s}/\sqrt{\text{h}}$
Output noise (no filtering)	0.8°/s rms	9 mg rms
Full-scale (FS) range	±350°/s	±18 g

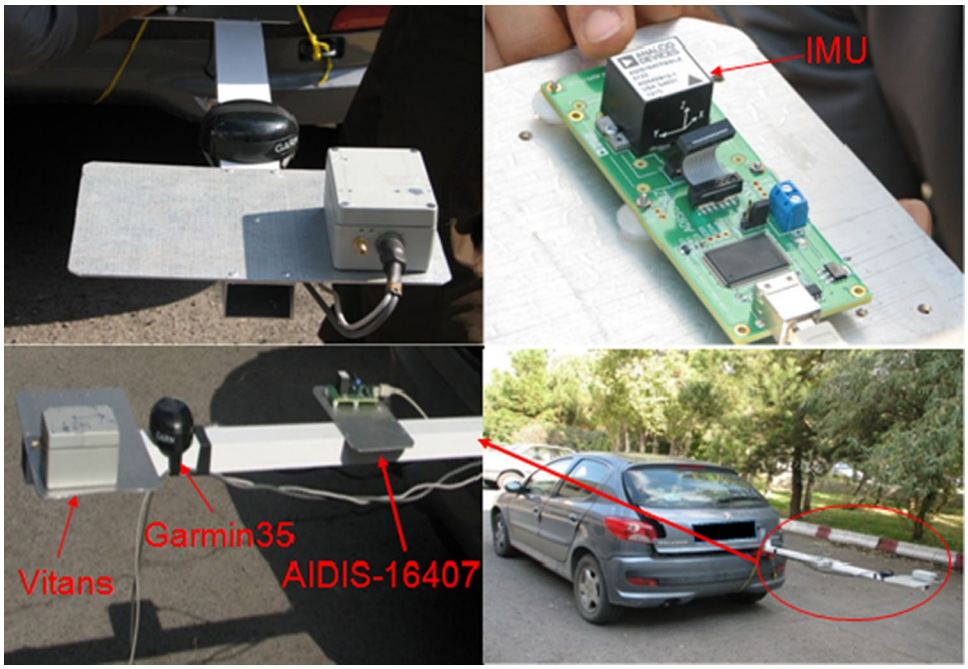

Fig. 3 Test equipment comprising ADIS-16407, Garmin-35, and Vitans system

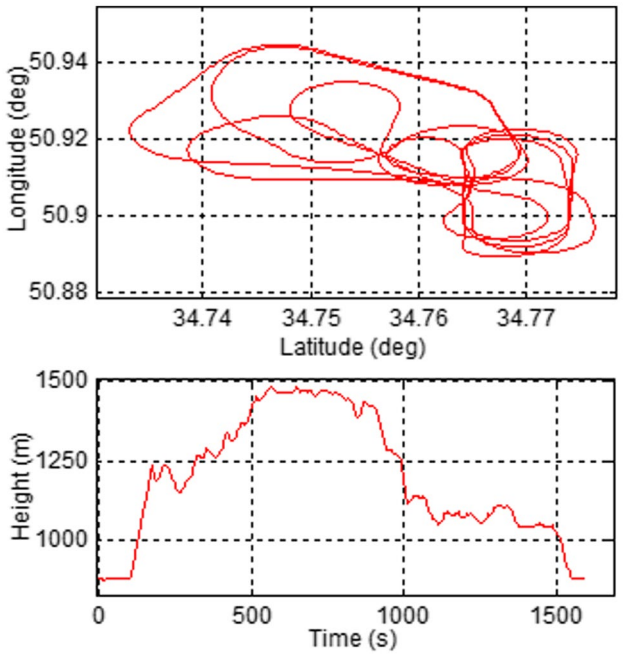

Fig. 4 Vehicle latitude–longitude and height trajectories during the flight test

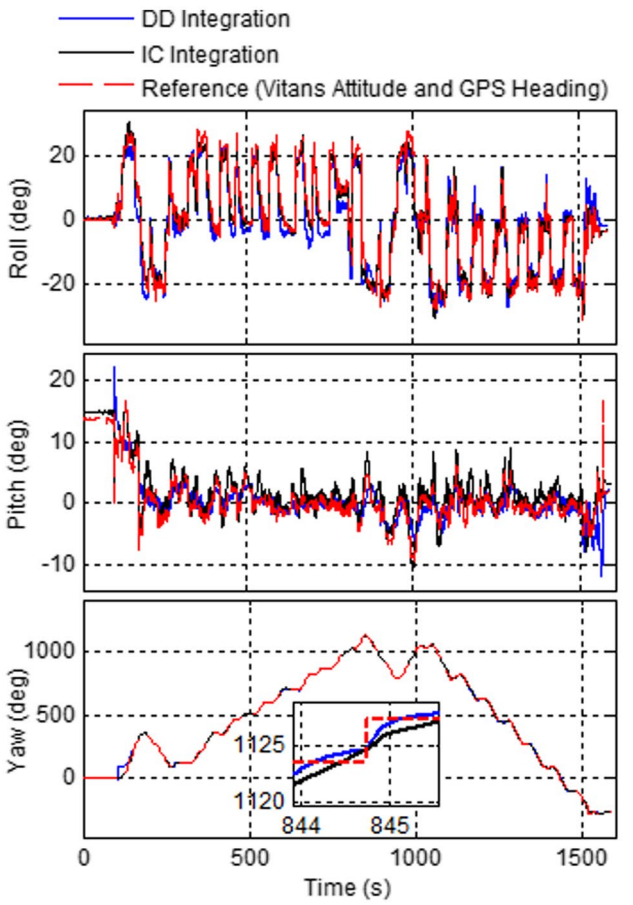

Fig. 5 Orientation estimation in comparison to Vitans attitude and GPS heading angle during the flight test

For better evaluation, the statistical characteristics such as mean and standard deviation of orientation estimation errors are gathered in Table 2. According to the standard deviation of estimation error, IC integration scheme leads to better accuracy in the attitude estimation, particularly for the roll angle. Due to using gravity attitude angles in the measurement vector of the estimation filter, the attitude

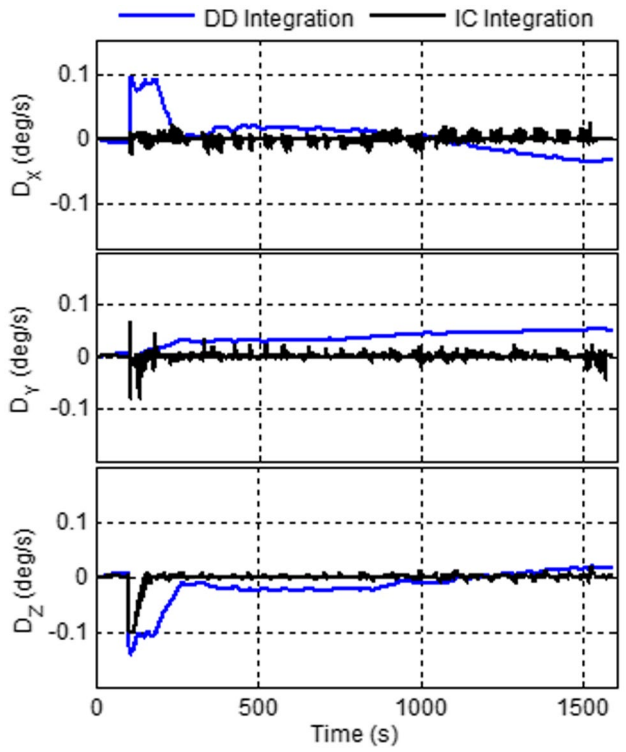

Fig. 6 Estimated gyroscope drift components in the b-frame

Table 2 Statistical analysis of the orientation estimation error in the flight test

Parameter	Mean value	Standard deviation ($\pm 1\sigma$)
DD integration		
Roll error (deg)	−0.80610	3.8500
Pitch error (deg)	0.13280	1.9080
Yaw error (deg)	−0.01757	0.9623
IC integration		
Roll error (deg)	−0.18550	2.0290
Pitch error (deg)	1.14500	1.3900
Yaw error (deg)	0.30510	3.0080

estimation of DD integrated INS/GNSS system slightly degrades in maneuvered dynamics with non-gravitational accelerations. The DD integration scheme has better accuracy in the heading estimation. However, it is more logical to evaluate the two algorithms during GNSS outages when there is no measurement for heading angle in the estimation filter.

The performance of the proposed IC and DD integrated INS/GNSS systems in the position and velocity estimation is

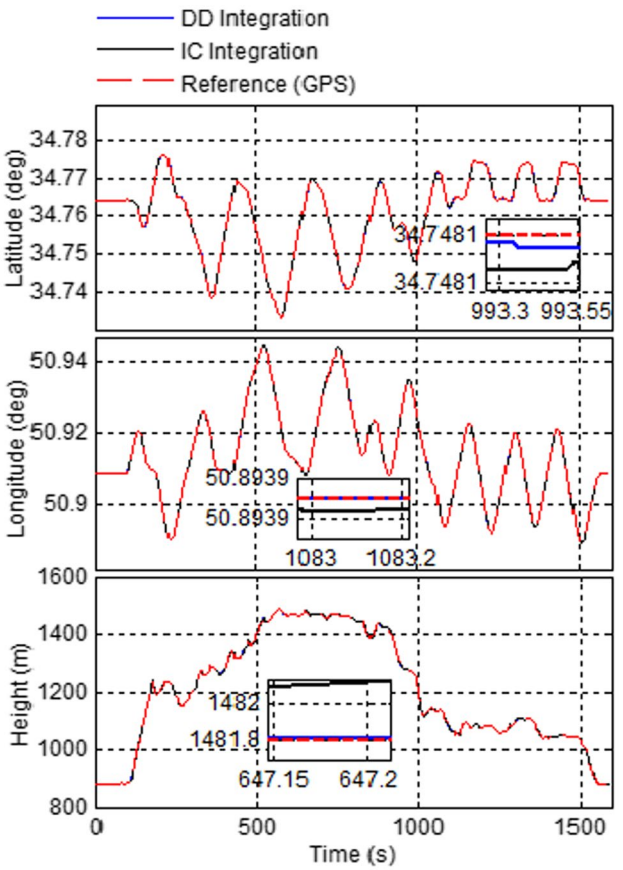

Fig. 7 Estimated latitude–longitude–height compared to GPS data during the flight test

shown in Figs. 7 and 8, respectively. As shown in the figures, both the IC and DD integrated INS/GNSS systems have a good performance in the position and velocity estimation. The long-term accuracy and reliability of the proposed algorithms are guaranteed. However, detailed assessment of the proposed INS/GNSS systems should be carried out during GNSS outages when there are no measurements for position and velocity components in estimation filters.

The proposed INS/GNSS systems are also assessed in land vehicular test. The land test has been executed for approximately 1050 s along a road. Geographical latitude–longitude and height trajectories during the land test are depicted in Fig. 9. The performance of the proposed IC and DD integrated INS/GNSS systems in orientation is shown in Fig. 10. The attitude angles obtained by the highly accurate Vitans system are used to evaluate the attitude estimation accuracy of the proposed algorithms. The estimated heading angle is evaluated in comparison to the GNSS heading angle. Table 3 summarizes the quantitative

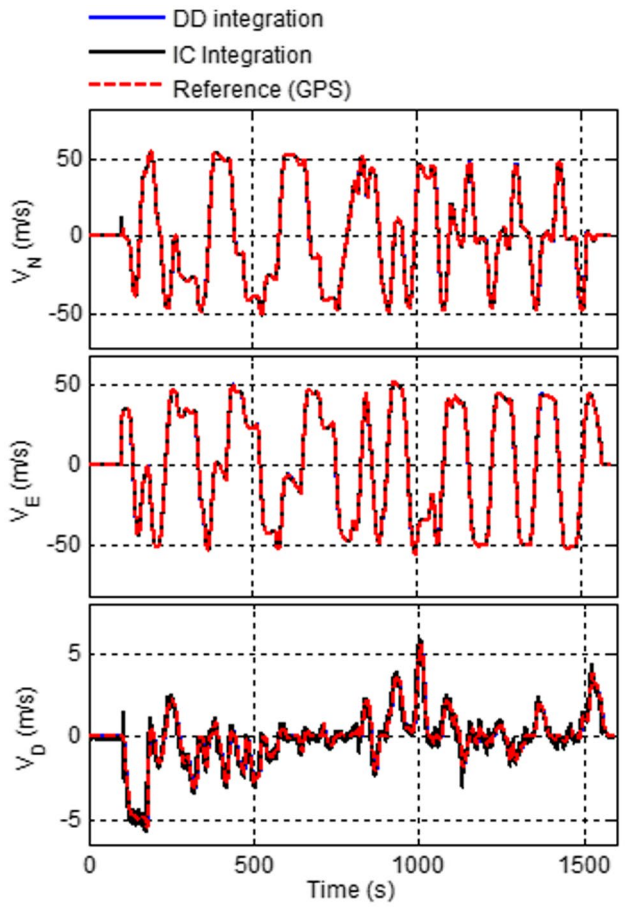

Fig. 8 Estimated velocity vector in the n-frame compared to GPS data during the flight test

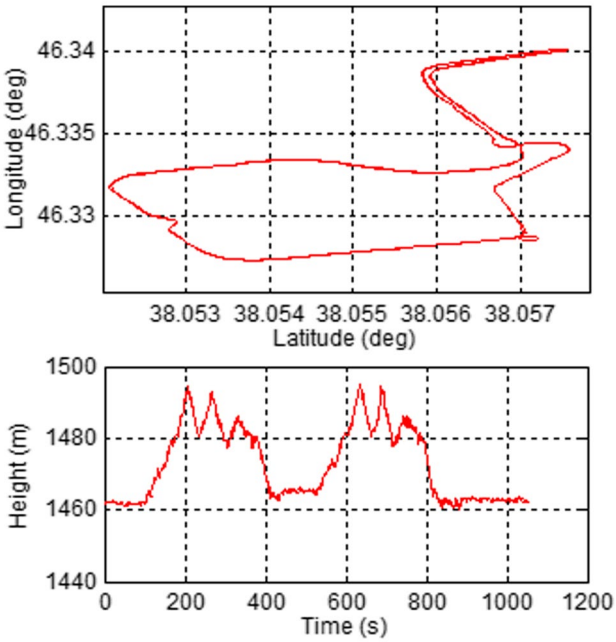

Fig. 9 Vehicle latitude–longitude and height trajectories during the land test

results of orientation estimation errors corresponding to each algorithm during the land test.

The land test also shows that the IC integrated INS/GNSS system has a better performance in attitude estimation compared to DD integrated system. As discussed previously, owing to using gravity attitude angles in the measurement vector of estimation filter, the attitude estimation of DD integrated INS/GNSS system degrades in maneuvered dynamics with non-gravitational accelerations.

The performance of the proposed INS/GNSS systems in the position and velocity estimation is shown in Figs. 11 and 12, respectively. According to the results of land vehicular test, both the IC integration and DD integration schemes have a reliable performance in the position, velocity, and heading estimation.

The main benefit of navigation integration concept consists in the availability of reliable navigation data during GNSS outages. Taking this into account, the following verifications have been conducted to assess the system performance during GNSS outages. The intervals of GNSS outage have been created artificially through the off-line analysis. The GNSS data existing in reality during these intervals were used as a reference. The intervals of GNSS outage during the flight test are [280–400] s and [520–820] s. The respective intervals for the land test are [300–420] s and [540–840] s. The attitude estimation accuracy of the proposed integration schemes during the intervals of GNSS outage in flight and land tests are illustrated in Figs. 13 and 14, respectively.

As the main advantage of the proposed integration schemes, the attitude estimation accuracy does not deteriorate during the long-time GNSS outages. Figures 15 and 16 show the heading angle estimation during GNSS outages in the flight and land tests, respectively. Quantitative results of heading estimation during the GNSS outages corresponding to these figures are summarized in Tables 4 and 5, respectively.

Quantitative results of Tables 4 and 5 show that the IC integration scheme yields more reliable navigation in heading angle estimation relative to the DD integration scheme. Furthermore, both the IC and DD integration schemes have a better performance in the land test. This arises from the fact that non-gravitational acceleration of a car vehicle is mainly generated along its longitudinal

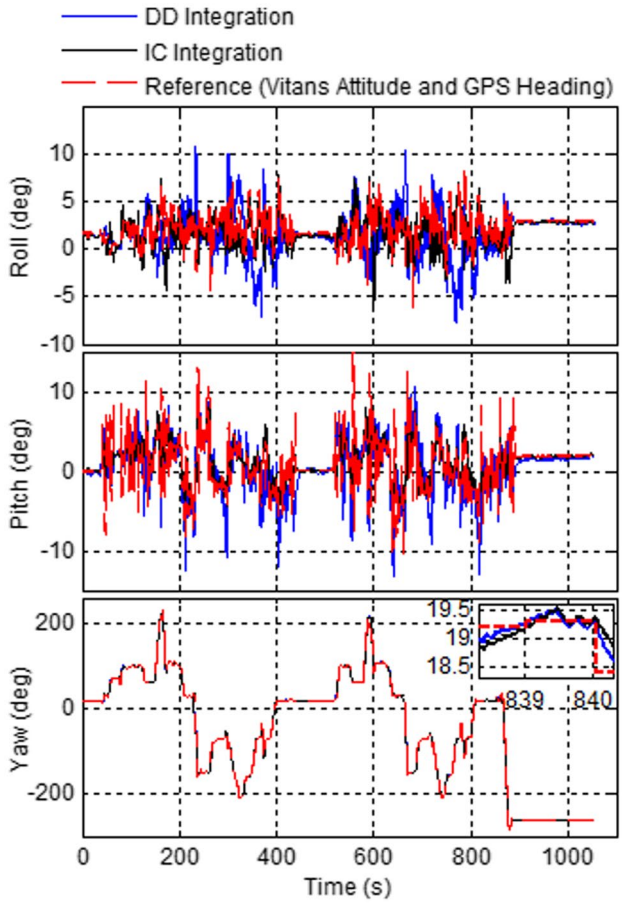

Fig. 10 Orientation estimation in comparison to Vitans attitude and GPS heading angle during the land test

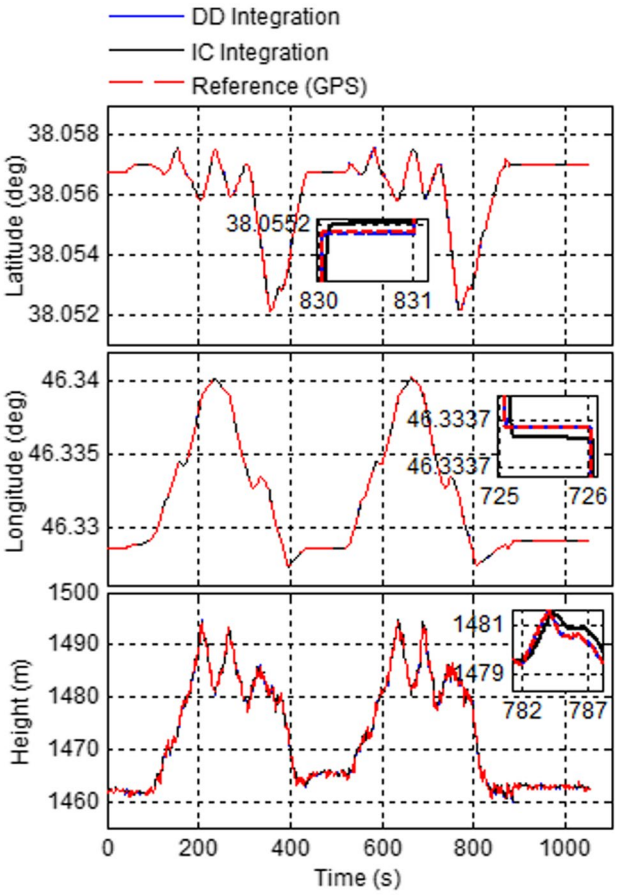

Fig. 11 Estimated latitude–longitude–height compared to GPS data during the land test

Table 3 Statistical analysis of the orientation estimation error in the land test

Parameter	Mean value	Standard deviation ($\pm 1\sigma$)
DD integration		
Roll error (°)	−0.65970	2.5130
Pitch error (°)	−0.43030	2.9650
Yaw error (°)	−0.01606	1.9200
IC integration		
Roll error (°)	−0.39550	1.1420
Pitch error (°)	−0.24090	2.0050
Yaw error (°)	−0.04152	2.1470

axis, but an airborne vehicle can be subjected to lateral dynamics. So, the vehicle undergoes higher maneuvering level in the flight test.

Non-gravitational acceleration effects are more crucial in DD integration scheme in which the gravity attitude is used in the measurement vector of estimation filter. In the IC integration scheme, in-run compensation of misalignment errors yields a corrected DCM matrix and consequently more accurate orientation estimation is achieved. Finally, it can be inferred from the experimental data that IC integration scheme results in better accuracy in orientation estimation compared to DD integration scheme.

Figures 17 and 18 show the estimation accuracy of velocity components during GNSS outages in flight test and land test, respectively. These figures clearly show that the proposed approach of auxiliary velocity-update based on NHC and ADV constraints provides appropriate measurements for velocity estimation during the long-time interval of GNSS outage in both the IC and DD integrated INS/GNSS systems. The results show that the proposed approach provides

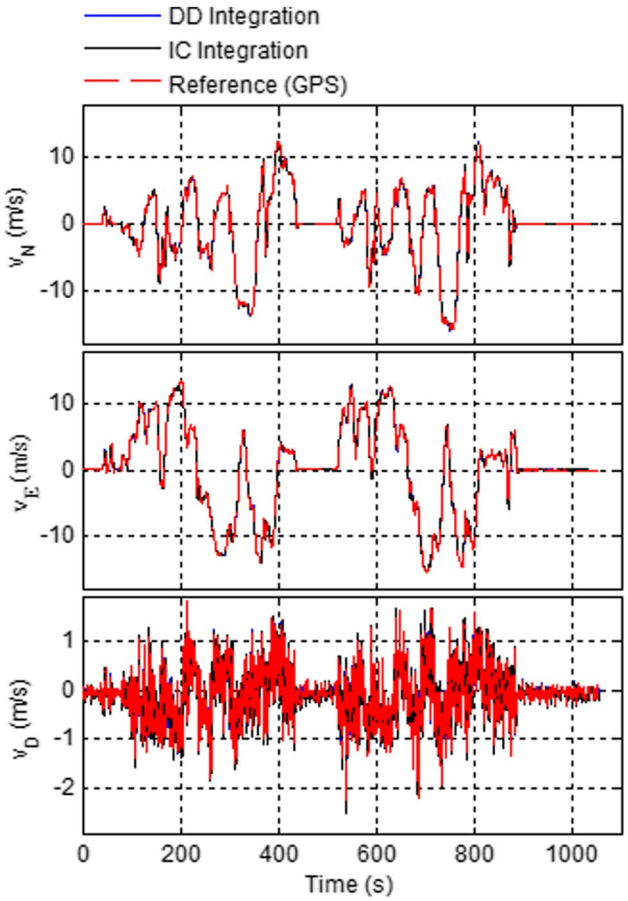

Fig. 12 Estimated velocity vector in the n-frame compared to GPS data during the land test

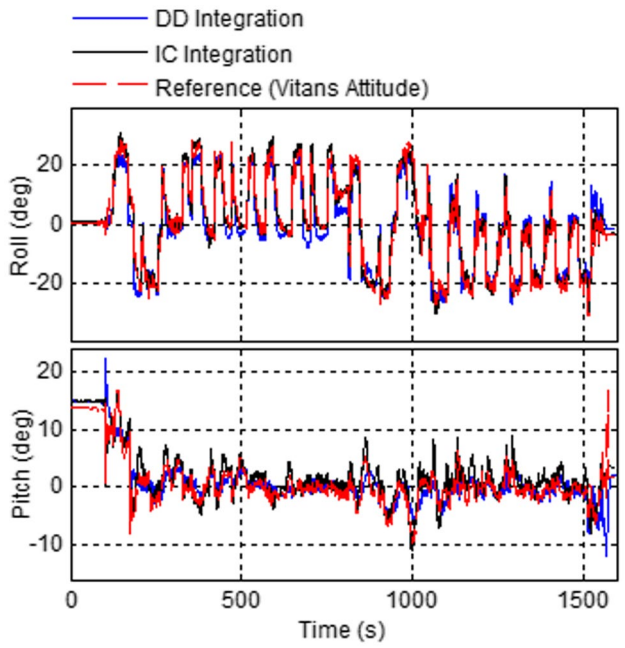

Fig. 13 Attitude estimation during the flight test with GNSS outage

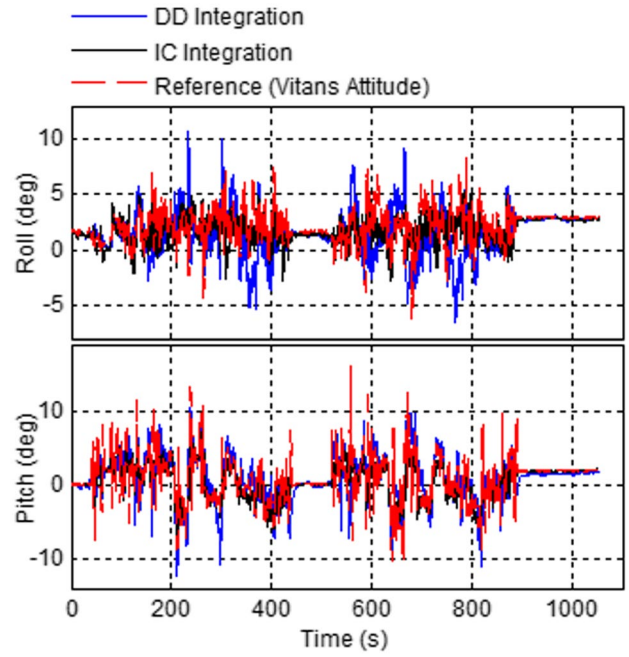

Fig. 14 Attitude estimation during the land test with GNSS outage

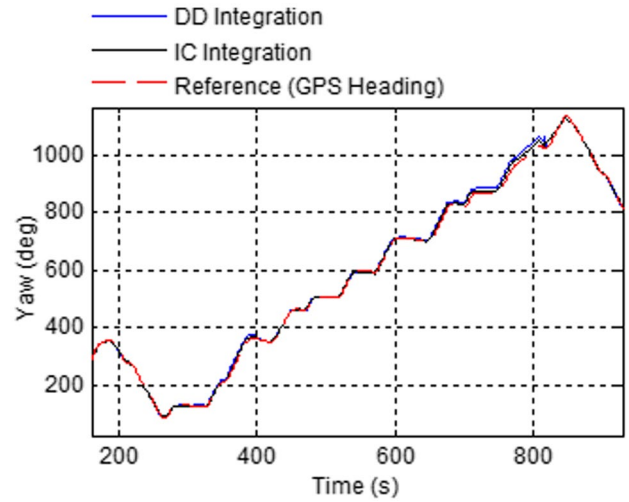

Fig. 15 Heading angle estimation during the flight test with GNSS outage

satisfying performance in velocity estimation during the periods of GNSS outage when the pure INS experiences very large error.

The performance of the proposed integration schemes in the position estimation during the GNSS outages is illustrated in Figs. 19 and 20. To give a better view, the estimation error of position components has been represented. The latitude and longitude errors have been expressed in meter based on the following relationships:

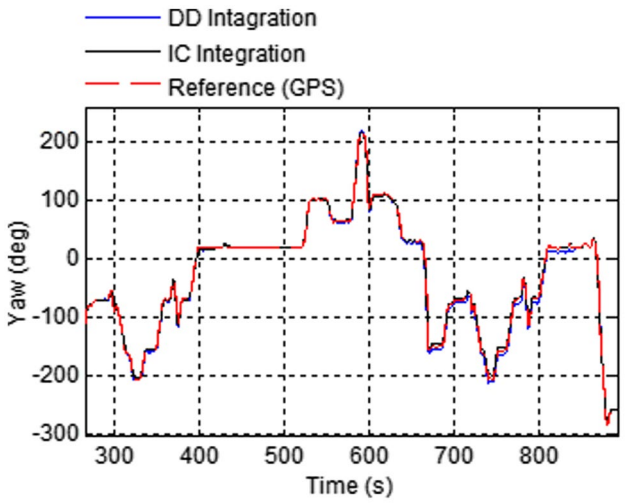

Fig. 16 Heading angle estimation during the land test with GNSS outage

Table 4 Heading estimation error at the last second of GNSS outage intervals in the flight test

Approach	GNSS outage [280–400] s	GNSS outage [520–820] s
Heading error		
IC integration	5.44°	9.11°
DD integration	12.33°	20.80°

Table 5 Heading estimation error at the last second of GNSS outage intervals in the land test

Approach	GNSS outage [280–400] s	GNSS outage [520–820] s
Heading error		
IC integration	4.29°	0.07°
DD integration	5.11°	7.20°

$$\begin{aligned}\text{Latitude error (m)} &= R_0 \times \text{Latitude error (rad)}\\ \text{Longitude error (m)} &= R_0 \times \text{Longitude error (rad)}\end{aligned} \quad (46)$$

where R_0 stands for the earth radius.

It is deduced from Figs. 19 and 20 that the DD integration scheme provides better position estimation during GNSS outages compared to IC integration scheme. The main reason behind this observation is that only small INS error are allowed due to the linearization process of deriving INS error dynamics in IC integration scheme. Therefore, the performance of the linear filter in the IC integration scheme slightly degrades when the INS error increases.

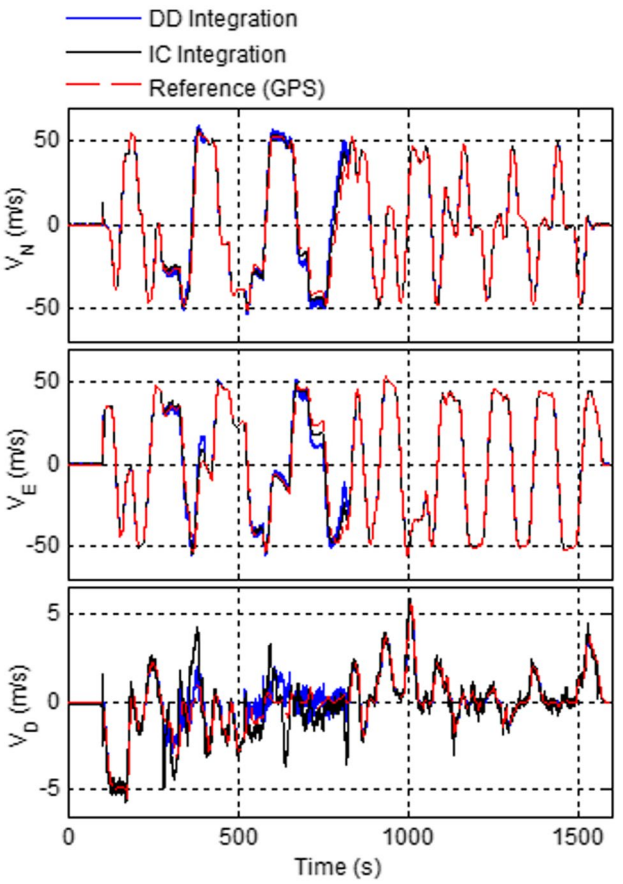

Fig. 17 Velocity estimation during the flight test with GNSS outage

To legitimize the assessment of the proposed approaches, the latitude error corresponding to proposed INS/GNSS systems are compared with that of the pure INS in Fig. 21. As shown in the figure, the position error of pure INS increases very rapidly. This is due to the large errors and uncertainties of the MEMS-grade IMU in low-cost INS. The figure clearly shows that the positioning error is noticeably controlled in the proposed INS/GNSS systems.

Conclusions

Motivated by improving navigation accuracy, reliability and long-term performance of low-cost INS/GNSS systems, this research introduced two approaches based on IC and DD integration schemes. The IC integration scheme relies on using INS error dynamics in the estimation

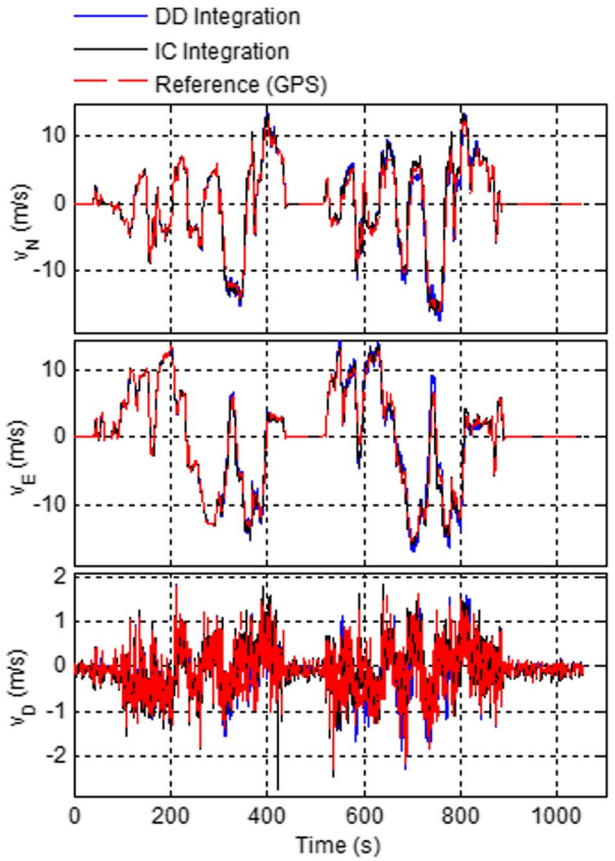

Fig. 18 Velocity estimation during the land test with GNSS outage

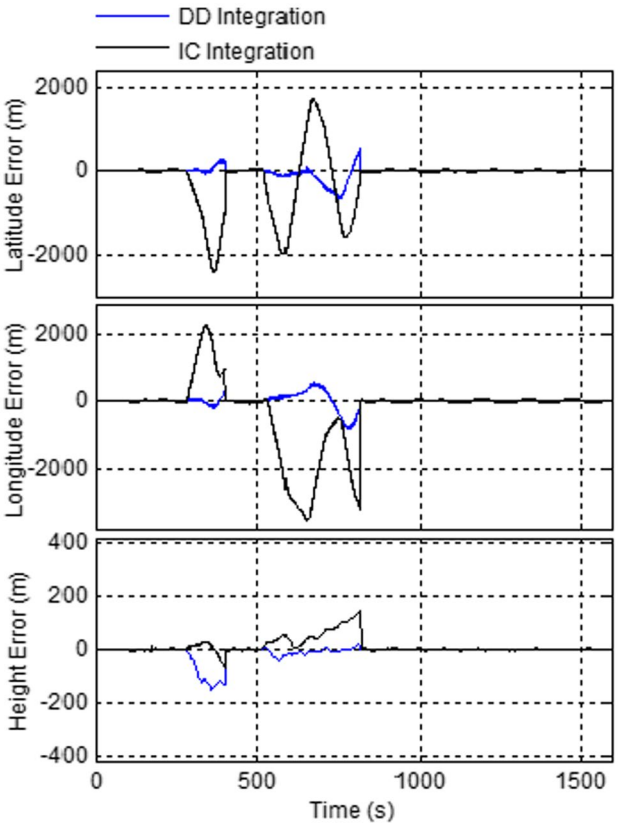

Fig. 19 Position estimation errors during the flight test with GNSS outage

process which is accomplished in a single central filter. The DD integration scheme relies on using basic nonlinear INS dynamics in the estimation process which is accomplished in two cascade filters. The proposed approaches have been assessed in flight and land vehicular tests. The results show a satisfying performance of the proposed approaches. One of the main challenges in the traditional INS/GNSS is system reliability and accuracy during the signal blockage of GNSS system. Considering this challenge, we proposed an auxiliary velocity-update approach containing NHC and ADV constraints. It has been shown that using auxiliary velocity-update brings about noticeable enhancement in the overall navigation accuracy and reliability for both the IC and DD integrated INS/GNSS systems during long periods of GNSS outage. An important remark deduced from the field tests is that IC integrated INS/GNSS has better accuracy in orientation estimation. But, when positioning accuracy is more crucial, DD integrated INS/GNSS should be preferred.

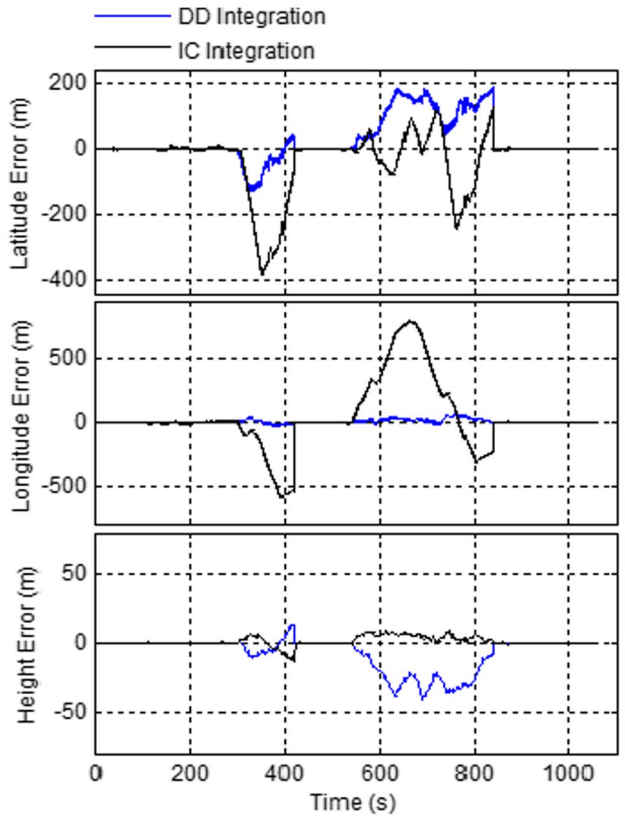

Fig. 20 Position estimation errors during the land test with GNSS outage

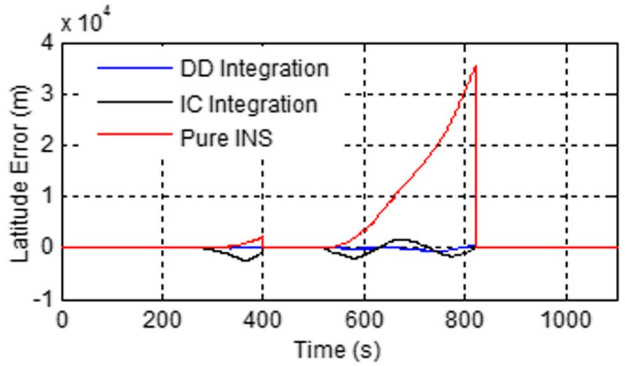

Fig. 21 Latitude error of the proposed INS/GNSS systems compared to pure INS

References

Ali J, Ushaq M (2009) A consistent and robust Kalman filter design for in-motion alignment of inertial navigation system. Measurement 42(4):577–582

Arasaratnam I, Haykin S (2009) Cubature Kalman filters. IEEE Trans Autom Control 54(6):1254–1269

Chang L, Hu B, Li A, Qin F (2013) Transformed unscented Kalman filter. IEEE Trans Autom Control 58(1):252–257

Chen X, Shen C, Zhang W-b, Tomizuka M, Xu Y, Chiu K (2013) Novel hybrid of strong tracking Kalman filter and wavelet neural network for GPS/INS during GPS outages. Measurement 46(10):3847–3854

Doostdar P, Keighobadi J (2012) Design and implementation of SMO for a nonlinear MIMO AHRS. Mech Syst Signal Process 32:94–115

Huang YW, Chiang KW (2008) An intelligent and autonomous MEMS IMU/GPS integration scheme for low cost land navigation applications. GPS Solut 12(2):135–146

Hwang DH, Oh SH, Lee SJ, Park C, Rizos C (2005) Design of a low-cost attitude determination GPS/INS integrated navigation system. GPS Solut 9(4):294–311

Keighobadi J (2011) Fuzzy calibration of a magnetic compass for vehicular applications. Mech Syst Signal Process 25(6):1973–1987

Meng Y, Gao S, Zhong Y, Hu G, Subic A (2016) Covariance matching based adaptive unscented Kalman filter for direct filtering in INS/GNSS integration. Acta Astronaut 120:171–181

Milanchian H, Keighobadi J, Nourmohammadi H (2015) Magnetic calibration of three-axis strapdown magnetometers for applications in MEMS attitude-heading reference systems. AUT J Model Simul 47(1):55–65

Musavi N, Keighobadi J (2015) Adaptive fuzzy neuro-observer applied to low cost INS/GPS. Appl Soft Comput 29:82–94

Nassar S, El-Sheimy N (2006) A combined algorithm of improving INS error modeling and sensor measurements for accurate INS/GPS navigation. GPS Solut 10(1):29–39

Noureldin A, El-Shafie A, Bayoumi M (2011) GPS/INS integration utilizing dynamic neural networks for vehicular navigation. Inf Fusion 12(1):48–57

Nourmohammadi H, Keighobadi J (2017) Decentralized INS/GNSS system with MEMS-grade inertial sensors using QR-factorized CKF. IEEE Sens J 17(11):3278–3287

Nourmohammadi H, Keighobadi J (2018) Fuzzy adaptive integration scheme for low-cost SINS/GPS navigation system. Mech Syst Signal Process 99:434–449

Rogers RM (2003) Applied mathematics in integrated navigation systems. American Institute of Aeronautics and Astronautics, Inc, Virginia

Simon D (2006) Optimal state estimation: Kalman, H ∞ and nonlinear approaches. John Wiley & Sons, Inc, New Jersey

Stančić R, Graovac S (2010) The integration of strap-down INS and GPS based on adaptive error damping. Robot Auton Syst 58(10):1117–1129

Titterton D, Weston JL (2004) Strapdown inertial navigation technology. The Institution of Engineering and Technology, IET, London

Hossein Nourmohammadi received the B.S. degree in Mechanical Engineering from Nooshirvani University of Technology, Babol, Iran, in 2010, the M.S. degree in Mechanical Engineering from Amirkabir University of Technology (Tehran Polytechnic), Tehran, Iran, in 2012 and Ph.D. degree in Mechanical Engineering at University of Tabriz, Iran, in 2017. He has been a Research Assistant with the Navigation, Guidance and Control laboratory at University of Tabriz since 2013. His current research interests include integrated navigation systems, estimation and identification, and nonlinear adaptive control.

Jafar Keighobadi received the B.S. degree in Mechanical Engineering from University of Tabriz, Tabriz, Iran, in 1997, M.S. and Ph.D. degrees in Mechanical Engineering and Control Systems from Department of Mechanical Engineering, Amirkabir University of technology (Tehran Polytechnic), Tehran, Iran, in 2000 and 2008, respectively. He is currently an Associate Professor of Mechanical Engineering Department, University of Tabriz. His research interests include artificial intelligence, estimation and identification, nonlinear robust control, and GNC.